Cellular/Molecular

High-Concentration Rapid Transients of Glutamate Mediate Neural–Glial Communication via Ectopic Release

Ko Matsui,[1] Craig E. Jahr,[1] and Maria E. Rubio[2]

[1]Vollum Institute, Oregon Health and Science University, Portland, Oregon 97239, and [2]Department of Physiology and Neurobiology, University of Connecticut, Storrs, Connecticut 06269

Until recently, communication from neurons to astrocytes was thought to be mediated by low-concentration transients of glutamate caused by spillover from the synaptic cleft. However, quantal events recorded in rat cerebellar Bergmann glial cells (BGs) have fast kinetics, comparable with those recorded in neurons. By combining outside-out patch recordings of BG AMPA receptors and quantitative electron microscopic analysis of glutamate receptor subunit 1 (GluR1) and GluR4 immunogold labeling measurements, at both the soma and membranes surrounding synapses, we estimate the absolute density of functional AMPA receptors. Using a kinetic model of BG AMPA receptors, we find that quantal events recorded in BGs are produced by high-concentration (~1–1.5 mM), fast transients (~0.5 ms decay) of glutamate, similar to transients within the synaptic cleft. Our results indicate that neural signaling to BGs is mediated by ectopic release of transmitter from presynaptic elements directly facing the BG membrane.

Key words: **Bergmann glial cell; Purkinje cell; glutamate; ectopic release; synaptic transmission; immunogold electron microscopy**

Introduction

Astrocytes in the CNS not only provide trophic support for neurons but also engage in bidirectional communication with neurons (Araque et al., 2001; Bezzi and Volterra, 2001). Signals from neurons to astrocytes initiate signaling cascades, including rises in intracellular Ca^{2+} concentration, which can either be restricted to local glial processes (Grosche et al., 1999) or propagate globally across many astrocytes (Newman, 2001). Such activation has been reported to cause astrocytes to release transmitters (Zhang et al., 2003), change their surface expression of receptors and transporters (Duan et al., 1999), or alter their morphologies (Iino et al., 2001).

Several transmitters used in neural–glial communication have been identified that initiate the signaling described above (Araque et al., 2001; Bezzi and Volterra, 2001). Glutamatergic transmission from neurons to astrocytes (Porter and McCarthy, 1996) was thought to be mediated by low-concentration (~10–200 μM), slow transients (lasting ~1–10 ms) of glutamate that spillover from the synaptic cleft (Bergles et al., 1997; Dzubay and Jahr, 1999). Because of this requirement for extended diffusion, such communication has been assumed to be a secondary effect of glutamatergic synaptic transmission between neurons.

In the cerebellum, both climbing fibers (CFs) and parallel fibers (PFs) make glutamatergic synapses on Purkinje cells (PCs) that drive postsynaptic AMPA receptors. Glutamate released from these fibers can also activate Ca^{2+}-permeable AMPA receptors on the surrounding astrocytes, the Bergmann glial cells (BGs) (Bergles et al., 1997; Clark and Barbour, 1997). Quantal responses to glutamate released from CFs and PFs can be recorded from BGs (Matsui and Jahr, 2003), and we found that these AMPA receptor-mediated responses have surprisingly fast kinetics that are comparable with the kinetics of quantal responses recorded in PCs. By combining patch recordings from the soma of BGs and quantitative electron microscopic analysis of glutamate receptor subunit 1 (GluR1) and GluR4 immunogold labeling measurements at both the soma and the membrane surrounding the synapse, we estimate the absolute density of functional AMPA receptors. By combining this density estimate with a kinetic model of BG AMPA receptors, we determined that quantal responses recorded in BGs are produced by high-concentration, fast transients of glutamate, similar to the glutamate transient in the synaptic cleft (Clements, 1996). In addition, clusters of AMPA receptors were found at BG membranes apposed to presynaptic elements. We suggest that ectopic release is necessary to activate low-affinity, Ca^{2+}-permeable AMPA receptors on BG membranes and provides a rapid form of transmission between neurons and astrocytes.

Materials and Methods

Tissue preparation for electrophysiological recordings. Parasagittal (250 μm) or coronal (350 μm) cerebellar slices from postnatal day 18 (P18)–P22 rats were used for the studies of CF-evoked and PF-evoked responses, respectively. Animals were anesthetized by inhalation of halothane and were decapitated, as approved by the Oregon Health and Science University Institutional Animal Care and Use Committee. Cerebella were cut with a vibroslicer (Leica, Nussloch, Germany) in ice-cold solution containing the following (in mM): 119.0 NaCl, 2.5 KCl, 2.0 $CaCl_2$, 1.3 $MgCl_2$, 1.0 NaH_2PO_4, 26.2 $NaHCO_3$, and 11.0 glucose (satu-

Received May 13, 2005; revised July 6, 2005; accepted July 7, 2005.

This work was supported by National Institutes of Health Grant NS40056 (C.E.J.) and the Research Foundation of the University of Connecticut (M.E.R.). We thank Jason Christie, John Harrison, Melissa Herman, Richard Piet, and Jacques Wadiche for valuable suggestions on the experiments and comments on this manuscript and Dr. R. J. Wenthold for kindly providing us with the antibodies for GluR1 and GluR4 subunits.

Correspondence should be addressed to Ko Matsui, Vollum Institute, Oregon Health and Science University, 3181 Southwest Sam Jackson Park Road, Portland, OR 97239. E-mail: matsuik@ohsu.edu.

DOI:10.1523/JNEUROSCI.1927-05.2005

 0270-6474/05/257538-10$15.00/0

rated with 95% O_2/5% CO_2). The slices were incubated in the same solution at ~34°C for 30 min and were then stored at room temperature. During the synaptic recordings, slices were superfused with the above solution with the addition of 100 μM picrotoxin, to block $GABA_A$ receptors. For BG recordings, 200 μM cyclothiazide (CTZ) was added to increase detection of BG quantal responses. All experiments, including both the synaptic experiments and outside-out patch experiments, were performed at 32–35°C attained using an in-line heating device (Warner Instruments, Hamden, CT).

Quantal response recording from slice preparations. Slices were visualized using 40× water-immersion objective on an Axioskop 2 FS upright microscope (Zeiss, Oberkochen, Germany) equipped with infrared-differential interference contrast. PCs were identified by their large cell body size (~20 μm) and BGs by their smaller cell body size, location in the PC layer, and low input resistance (~20–40 MΩ). Whole-cell recordings were made with a MultiClamp 700A patch-clamp amplifier (Molecular Devices, Union City, CA). Signals were filtered at 2–4 kHz and digitized at 20–100 kHz with an ITC-18 interface (InstruTech, Port Washington, NY) and collected using acquisition software written by J. S. Diamond in IgorPro software (WaveMetrics, Lake Oswego, OR). Pipettes with resistances of 1–2 or 2–3 MΩ were used for recordings from PCs and BGs, respectively. Series resistance was compensated ~80% for PC recordings but not for BG recordings. PCs were typically voltage clamped at −70 mV and BGs at −65 to −70 mV. CFs were stimulated in parasagittal slices with a theta glass pipette filled with bath solution placed in the granule cell layer using a constant voltage-isolated stimulator (20–100 μs pulse of 10–99 mV; one to five stimuli at 20 Hz; Digitimer, Welwyn Garden City, UK). The pipette position and stimulus intensity were adjusted until the voltage necessary to produce an all-or-none response was minimized. PFs were stimulated in coronal slices with the stimulating electrode placed in the molecular layer (one to five stimuli at 50 Hz).

To desynchronize exocytotic events, divalent concentrations were changed to 0.5 mM Sr^{2+}/2.8 mM Mg^{2+} or 1.0 mM Sr^{2+}/1.3 mM Mg^{2+} for CF–PC recordings and 5 mM Sr^{2+} for CF–BG recordings. Pipette solutions contained the following (in mM): 35 CsF, 100 CsCl, 10 HEPES, and 10 EGTA for PC recordings and 82 $CsCH_3SO_3$, 40 CsCl, 20 HEPES, 10 HEDTA, and 3 $BaCl_2$ for BG recordings. All pipette solutions were titrated to pH 7.2 with CsOH. The sources of the chemicals are as follows: picrotoxin was from Sigma (St. Louis, MO); CTZ was from Tocris Cookson (Ellisville, MO).

Outside-out patch experiments. A theta glass flow-pipette (fabricated from borosilicate glass capillary tubing TG150–4; Warner Instruments) was mounted on a piezoelectric bimorph (Morgan Matroc, Bedford, OH) and used for agonist application to outside-out patches. Solution exchange times were measured after each experiment by rupturing the patch and recording junction currents across the open pipette tip (open tip response; 20–80% exchange rate, ~200 μs). Different concentrations of agonist were applied on individual patches by connecting a four-barrel miniature manifold (Warner Instruments) to one compartment of the theta glass pipette. Solution exchange for different concentrations was determined by measuring the 0.1–99.9% change in junction current amplitude after switching solutions (~20 s). The solutions were allowed to flow for ~30–60 s between conditions to allow complete exchange. The external solution used for agonist applications contained the following (in mM): 140.0 NaCl, 2.0 $CaCl_2$, 1.3 $MgCl_2$, and 5.0 HEPES, pH adjusted to 7.4 with NaOH.

Data analysis and AMPA receptor channel simulations were performed using Axograph 4.6 (Molecular Devices), and statistical analysis was performed using Microsoft Excel (Microsoft, Redmond, WA). Reported values in text are given as mean ± SD.

Tissue preparation for electron microscopy. For structural analysis (see Fig. 7), brain tissue was fixed by two methods to control for fixation artifacts. Four P21 Sprague Dawley rats were anesthetized with a mixture of 60 mg/kg ketamine and 6.5 mg/kg xylazine. After checking anesthetic depth, two animals were perfused with cold oxygenated artificial CSF (ACSF) for 30 s, the other two with 4% paraformaldehyde and 0.5% glutaraldehyde in 0.12 M phosphate buffer, pH 7.2, for 10 min. Brains perfused with ACSF were rapidly removed, sliced with a vibratome, immersion fixed in 2% paraformaldehyde and 1.25% glutaraldehyde in sodium cacodylate buffer, pH 7.2, for 2 h, washed in buffer, and postfixed with 1% osmium tetroxide. Tissues were then flat embedded in epoxy resins (Rubio and Wenthold, 1997). Glutaraldehyde fixation and postfixation with osmium were used in this method to fix bilipid membranes, which allows high-contrast imaging of cell structures. Additionally, immersion fixation was used instead of vascular perfusion to prevent possible reorganization of membrane structure by the rapid circulatory delivery of the fixative to the brain. Brains perfused with fixative were removed, immersion fixed for an additional hour at 4°C, rinsed in buffer, and stored overnight at 4°C. Low glutaraldehyde fixation was then followed by cryoprotection in glycerol and cryofixation in propane at −185°C. Subsequently, cerebellar regions were dissected and processed for freeze substitution and low-temperature embedding, as described previously by Rubio and Wenthold (1997, 1999). As the sample warms from −90°C in methanol, ice is replaced by fixative; this method results in less shrinkage and less movement of soluble elements. A portion of this perfusion-fixed tissue was processed further for postembedding immunogold labeling (see Figs. 4, 5). In all cases, cerebellar sections were taken from the cerebellar folia III–V to eliminate variations attributable to regional differences in cerebellar structure/function and to differences in timing of ontogenesis (Takayama et al., 1996).

Postembedding immunogold labeling procedure after freeze substitution. Cerebellar regions were dissected and processed for freeze substitution and low-temperature embedding as described above (Rubio and Wenthold, 1997, 1999). Postembedding immunogold labeling of GluR1 and GluR4 AMPA receptor subunits in perfusion-fixed tissue followed a protocol similar to that described previously by Rubio and Wenthold (1997, 1999) and Rubio and Soto (2001). Well characterized, affinity-purified polyclonal antibodies for GluR1 and GluR4 (Wenthold et al., 1992) were used at 2 μg/ml and labeled with 5-nm-diameter colloidal gold particles coupled to secondary antibodies (Amersham Biosciences, Piscataway, NJ). Colocalization of GluR1 and GluR4 receptor subunits was performed with double-postembedding immunogold labeling using paraformaldehyde vapors between two sequential immunogold labeling procedures. Two sizes of gold particles conjugated secondary antibodies were used (10 nm for GluR1 and 5 nm for GluR4). Controls included omitting the primary antibody in the first and sequential immunogold labeling and preadsorption of primary antibody with the corresponding peptide conjugate (Rubio and Wenthold, 1997, 1999).

Electron microscopy was also performed with the GluR1 antibody obtained from Upstate Cell Signaling Solutions (Charlottesville, VA), with essentially the same results (data not shown). Electron micrographs were taken at 34,300× magnification with a Philips (Aachen, Germany) 300M transmission electron microscope (TEM) and scanned at a resolution of 1600 dots per inch (dpi) using an Epson Expression 1680 scanner (Epson America, Long Beach, CA). Image processing was performed with Adobe Photoshop (Adobe Systems, San Jose, CA) using only the brightness and contrast commands to enhance gold particles.

Neuron–glia distribution of gold particles for GluR1 and GluR4. Electron microscopic (EM) identification of PF and CF synapses on PCs was based on defined criteria (Mugnaini, 1972; Palay and Chan-Palay, 1974; Altman and Bayer, 1997; Zhao et al., 1998; Rubio and Soto, 2001). PF–PC synapses have small and globular axonal varicosities containing a loose collection of round synaptic vesicles. These varicosities form asymmetrical synapses (gray type I) with the spines of spiny branchlets of PC dendrites. CF varicosities are large, filled with round clear synaptic vesicles, and form asymmetrical synapses with dendritic spines and larger dendritic shafts of PCs. They differ from PF not only in the locus of termination but also in that synaptic vesicles are less regular in their shape, size, and distribution (Altman and Bayer, 1997). Synapses that could not be clearly identified by the above criteria were not included in the analysis. BG processes were identified by their irregular, stellate shape and by the presence of glycogen granules and bundles of intermediate filaments in a relatively clear cytoplasm (Palay and Chan-Palay, 1974; Peters et al., 1991; Rubio and Soto, 2001).

Quantitative evaluation of GluR1 and GluR4 receptor immunolabeling. The distribution and relative density of the GluR1 and GluR4 subunit immunolabeling in the BG was determined for 124 synapses (PF, 100;

CF, 24) and 120 synapses (PF, 100; CF, 20), respectively. A total of 230 (GluR1) and 243 (GluR4) gold particles were counted. The distance between the center of each gold particle and the outer leaflet of the BG plasma membrane facing and not facing the presynaptic ending and/or dendritic spine was measured. The neuron–glial cell axis was divided into 5 nm bins, and each gold particle was assigned to one bin. All gold particles located within 180 nm from the outer leaflet of the BG membrane were included in the analysis. In addition, the linear density of gold particles was computed using NIH Scion Image for each BG profile by dividing the number of gold particles in a BG profile by the membrane length of that profile. The average linear density was computed across all profiles.

To determine the distribution of clusters of gold particles at BG membranes we divided the gold particles in two groups, those formed by one or two and by three to six particles. The percentage of the two groups was related to the total population of gold particles (GluR1, $n = 215$ gold particles; GluR4, $n = 150$). The Student's t test (two-tailed sample assuming unequal variances) was used to determine the significance ($p < 0.05$) of the sample.

Neuron–glia plasma membrane distance. Both immersion-fixed cerebella and perfusion-fixed cerebella followed by freeze substitution (as described above) were used to compare the extracellular distance between BG and PF membrane appositions and the width of PF–PC synaptic clefts. Only synapses with well defined synaptic clefts and appositions with well defined plasma membranes were analyzed ($n = 50$ for each condition). Measurements were taken randomly along lengths of BG–PF appositions and within synaptic clefts (six measurements per apposition/cleft). NIH Scion Image software was used for all measurements. Electron micrographs were taken at 50,000× magnification with a Philips 300M TEM and scanned at a resolution of 1600 dpi using an Epson Expression 1680 scanner.

Results

Quantal events in PCs and BGs have similar time courses

Quantal events evoked by stimulation of either CFs or PFs were recorded from PCs of juvenile rats (P18–P22) in acute cerebellar slices at ~32–35°C (Fig. 1*A*,*B*). To observe quantal events after CF stimulation, Sr^{2+} was substituted for extracellular Ca^{2+} (Xu-Friedman and Regehr, 2000). Asynchronous, as well as synchronous, release occurs from PFs in physiological Ca^{2+} concentrations (Atluri and Regehr, 1998). We used single or multiple CF or PF stimuli to induce asynchronous release.

Quantal events were similarly evoked in BGs in the presence of CTZ (200 μM) (Fig. 1*C*,*D*). We have shown that BG quanta evoked in the presence of CTZ were slower than those in control solutions (Matsui and Jahr, 2003) but occurred with higher frequency because of the increased peak open probability of AMPA receptors in CTZ (Dzubay and Jahr, 1999). Despite the slowing of BG quanta by CTZ, the rise times of quanta in BGs and PCs (in the absence of CTZ) were similar, although the peak conductance of BG events was less than one-half of that of events in PCs (Fig. 1*E*). The following experiments were done to determine the amplitude and the time course of the glutamate transient underlying quanta recorded in BGs.

Kinetic properties of BG AMPA receptors in outside-out patches

AMPA receptor currents in outside-out patches from BGs were activated with rapid applications of glutamate in the presence of CTZ to block AMPA receptor desensitization (32–35°C). The dose–response relationship of glutamate activation of BG AMPA receptors was obtained by applying a range of concentrations of glutamate (Fig. 2*A*). The AMPA receptor responses were fitted with the Hill equation (Fig. 2*B*) scaled by the maximum open probability (P_{Omax}) determined below. The EC_{50} was ~248 μM and 10 mM glutamate produced a saturating response. As expected of ligand-gated ion channels, higher concentrations of glutamate evoked currents with shorter rise times but had no effect on their decay times (Fig. 2*C*). Based on the relationship between the 20–80% rise time and the glutamate concentration (Fig. 2*D*), patch responses evoked by ~4–6 mM of glutamate would give a 20–80% rise time similar to the rise time of the quantal response (~192–224 μs). However, this comparison results in an upper estimate of the glutamate transient underlying the quantal events, because extremely short pulses of a wide range of glutamate concentrations will result in responses with similar kinetics, although very different peak P_O values. We therefore examined the P_O, the single-channel conductance (γ), and the density of BG AMPA receptors.

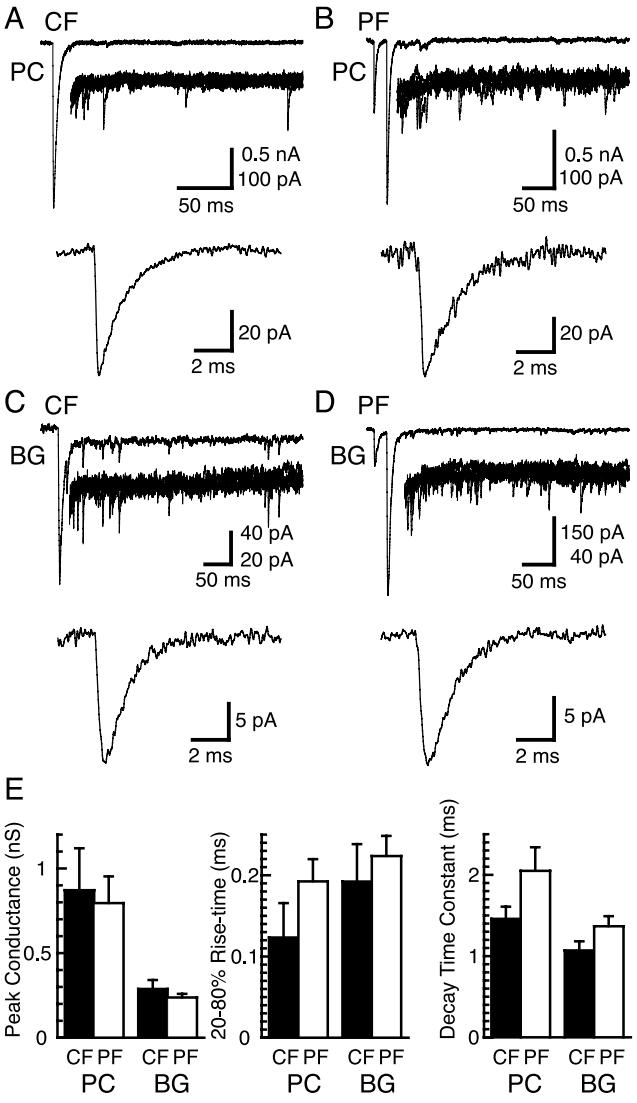

Figure 1. Kinetics of quantal events in Purkinje cells and Bergmann glial cells. ***A***, CFs stimulated in the presence of 1.0 mM Sr^{2+}/1.3 mM Mg^{2+} evoked asynchronously occurring quantal events in voltage-clamped PCs ($V_h = -70$ mV). Top trace, Example of a single epoch; middle traces, superimposition of the asynchronous events of five epochs at higher gain; bottom trace, average waveform of quantal responses collected from this cell. ***B***, PC responses, as in ***A***, after two PF stimuli (20 ms interval) in the presence of 2.0 mM Ca^{2+}/1.3 mM Mg^{2+}. ***C***, BG responses to CF stimulation in the presence of 5 mM Sr^{2+} and 200 μM CTZ ($V_h = -65$ mV). ***D***, BG responses to two PF stimuli (20 ms interval) in the presence of 2.0 mM Ca^{2+}/1.3 mM Mg^{2+} and 200 μM CTZ. ***E***, Summary of the peak conductance, the 20–80% rise time, and the decay time constant of quantal events recorded from PCs and BGs by stimulation of CFs and PFs ($n = 5$, 6, 4, and 7 cells for CF–PC, PF–PC, CF–BG, and PF–BG responses, respectively). Error bars represent SD.

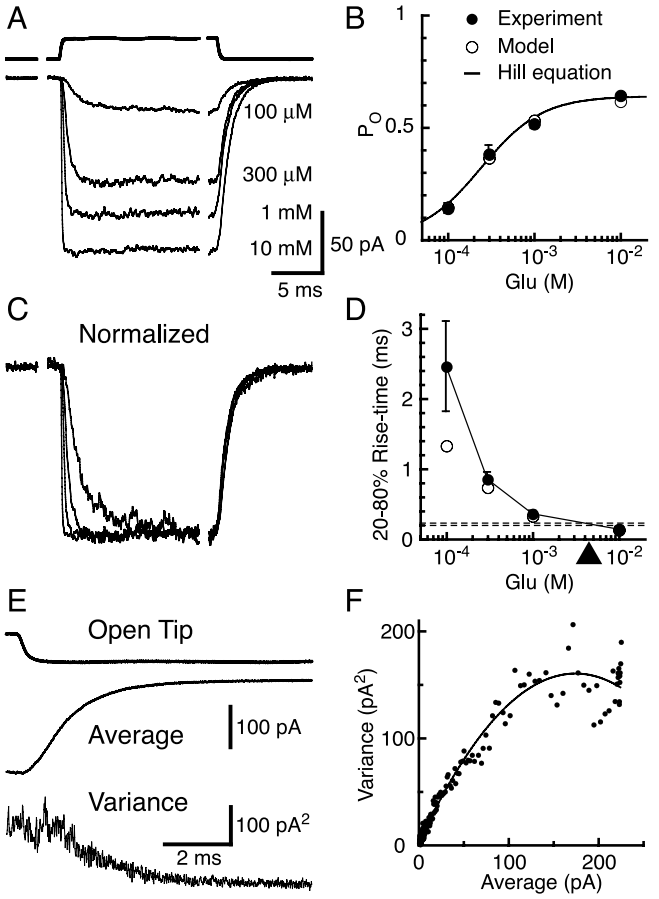

Figure 2. AMPA receptor responses in outside-out patches from BGs. ***A***, Responses of outside-out patches from BG soma to rapid application of 100 μM to 10 mM glutamate (bottom 4 traces). Top trace, Open tip junctional current indicating the time course of solution exchange. All patch recordings were done in the presence of 200 μM CTZ. $V_h = -70$ mV. ***B***, Dose–response curve normalized by responses to 10 mM glutamate. Two or more concentrations of glutamate were tested in each patch, and the amplitudes were normalized to the response to 10 mM glutamate. Response amplitude at 10 mM glutamate was set to a P_0 of 0.64 as calculated by nonstationary noise analysis from separate set of patches as in ***E*** and ***F***. Each filled circle is from eight or nine patches. The average data were fitted with the Hill equation (solid line; $V_{max} = 0.64$; $K_D = 248$ μM; $n = 1.2$). Open circles are from the kinetic model in Figure 8*A*. ***C***, Patch responses, shown in ***A***, normalized to their peak amplitudes. ***D***, Rise times (20–80%) of the patch responses versus glutamate concentration. Horizontal dashed lines represent the averages of the rise time of quanta recorded from CF (bottom) and PF (top) stimulations. The arrowhead indicates the approximate concentration of square pulses of glutamate needed to evoke patch currents with the same rise time. Filled circles, Data from 8–11 patches. Open circles are from the kinetic model in Figure 8*A*. ***E***, The decaying phase of the patch responses to 10 mM glutamate was used for the nonstationary noise analysis. Top trace, Open tip response; middle trace, average glutamate response; bottom trace, ensemble variance for 73 sweeps. ***F***, The variance is plotted against the mean current from the same patch as in ***E***. Each data point represents an average of five neighboring sampling points. A parabolic function (solid line) was fitted to the data and the single-channel conductance, the number of channels in the patch, and P_{0max} was extracted (26.0 pS; 192 channels; $P_{0max} = 0.64$ for this patch). Error bars represent SD.

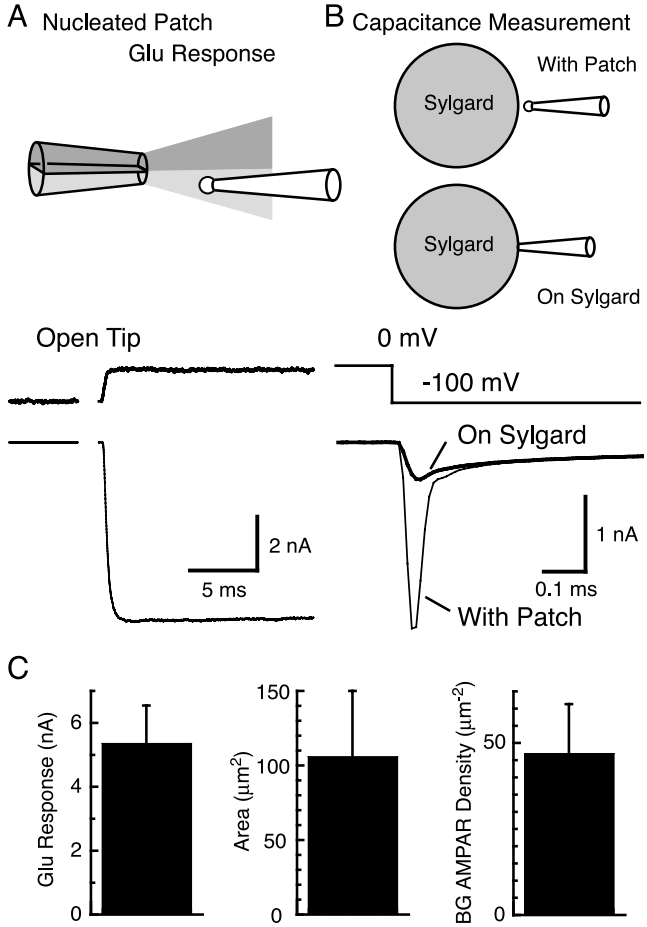

Figure 3. Density of AMPA receptors at the cell soma of BGs. ***A***, Nucleated outside-out patches were taken from the soma of BGs by applying slight negative pressure inside the pipette while pulling the pipette away from the cell soma. Rapid application of 10 mM glutamate in the presence of 200 μM CTZ (top trace, open tip junctional current) resulted in large AMPA receptor-mediated currents (bottom trace). $V_h = -70$ mV. ***B***, The same nucleated outside-out patches used for recording glutamate responses were used for capacitance measurements. Voltage steps of −100 mV were applied, and the resulting current responses were recorded (thin line, with patch). After touching the surface of a Sylgard bead, the capacitive current attributable to the patch disappeared (thick line, on Sylgard). The difference between the two currents was taken. Step response of the recording system to the same voltage pulses were determined by recording the response of a resistor connected to the head-stage of the patch amplifier. This trace was fitted to the final level of the leakage component. Subtraction of this leakage component leaves the capacitive current across the membrane patch. The membrane charge induced by the voltage pulse is given by the integration of this capacitive current (90.7 fC for this patch). ***C***, Left, Summary of glutamate response amplitudes from nucleated outside-out patches. Middle, Area of the membrane calculated from the capacitive charge. Right, BG AMPA receptor (AMPAR) density calculated by dividing glutamate response amplitude by the membrane potential, P_{0max}, and single-channel current of BG AMPA receptors ($n = 6$ patches). Error bars represent SD.

AMPA receptor properties and density at the BG soma

Using the decay phase of the patch currents evoked by a saturating concentration of glutamate (10 mM), nonstationary noise analysis (Sigworth, 1980) was used to estimate the P_{Omax} and γ of BG AMPA receptors in outside-out patches (Fig. 2*E*,*F*). P_{Omax} and γ were calculated for each patch and then averaged ($P_{Omax} = 0.64 \pm 0.08$; $\gamma = 26.6 \pm 6.5$ pS; $n = 13$ patches). These values are similar to those found for Ca^{2+}-permeable AMPA receptors from dentate basket cells (Koh et al., 1995).

We next used nucleated outside-out patches (Sather et al., 1992) taken from BG somata to obtain large areas of membrane. Responses of nucleated patches to glutamate (10 mM) were much larger than those of conventional outside-out patches (Fig. 3*A*) (5.4 ± 1.2 nA vs 116 ± 75 pA; $n = 6$ and 13; $V_h = -70$ mV). The number of functional AMPA receptors on the patch membrane was determined by dividing the amplitude of the glutamate response by the single-channel current and the P_{Omax} (4484 ± 1552 channels).

After recording the glutamate response, the membrane capacitance of the same nucleated patches was measured (Fig. 3*B*) (Karpen et al., 1992). The nucleated patches were charged with

−100 mV voltage pulses, and the resulting capacitive currents were measured. The patch electrode was then pressed against a Sylgard bead to eliminate the patch-membrane capacitance and replace the membrane resistance with the large resistance formed between the tip of the pipette and the Sylgard bead. The difference in current flow between these two conditions represents the charge required to alter the patch membrane potential by 100 mV. Using the specific membrane capacitance (1 $\mu F/cm^2$) (Hille, 2001), we estimated that the membrane area of the nucleated patches (Fig. 3*C*) (106 ± 43 μm^2; $n = 6$ patches). Dividing the number of functional AMPA receptors in each membrane patch by the membrane area gives the AMPA receptor density at BG soma (Fig. 3*C*) (47 ± 19 receptors/μm^2; $n = 6$ patches).

The same approach was applied to PC somatic patches. We estimated the single-channel conductance (14.3 ± 2.4 pS) and the P_{Omax} (0.66 ± 0.09; $n = 3$ patches) from conventional outside-out patches and the density of AMPA receptors (2.8 ± 1.2 receptors/μm^2; $n = 7$ patches) from PC nucleated patches (all in the presence of CTZ). The density of functional AMPA receptors at BG somata is ~17-fold higher than that at PC somata. However, BG AMPA receptor density is still much lower than that at PC postsynaptic density (PSD) (~1000 receptors/μm^2) (Momiyama et al., 2003; Tanaka et al., 2005).

We have estimated the density of functional AMPA receptors at the soma of BG. However, we do not know whether the density of receptors at the membrane surrounding the synapse is different from that at the cell soma. Therefore, we performed quantitative immunogold EM analysis to measure the relative glutamate receptor density difference between the regions of BG membrane.

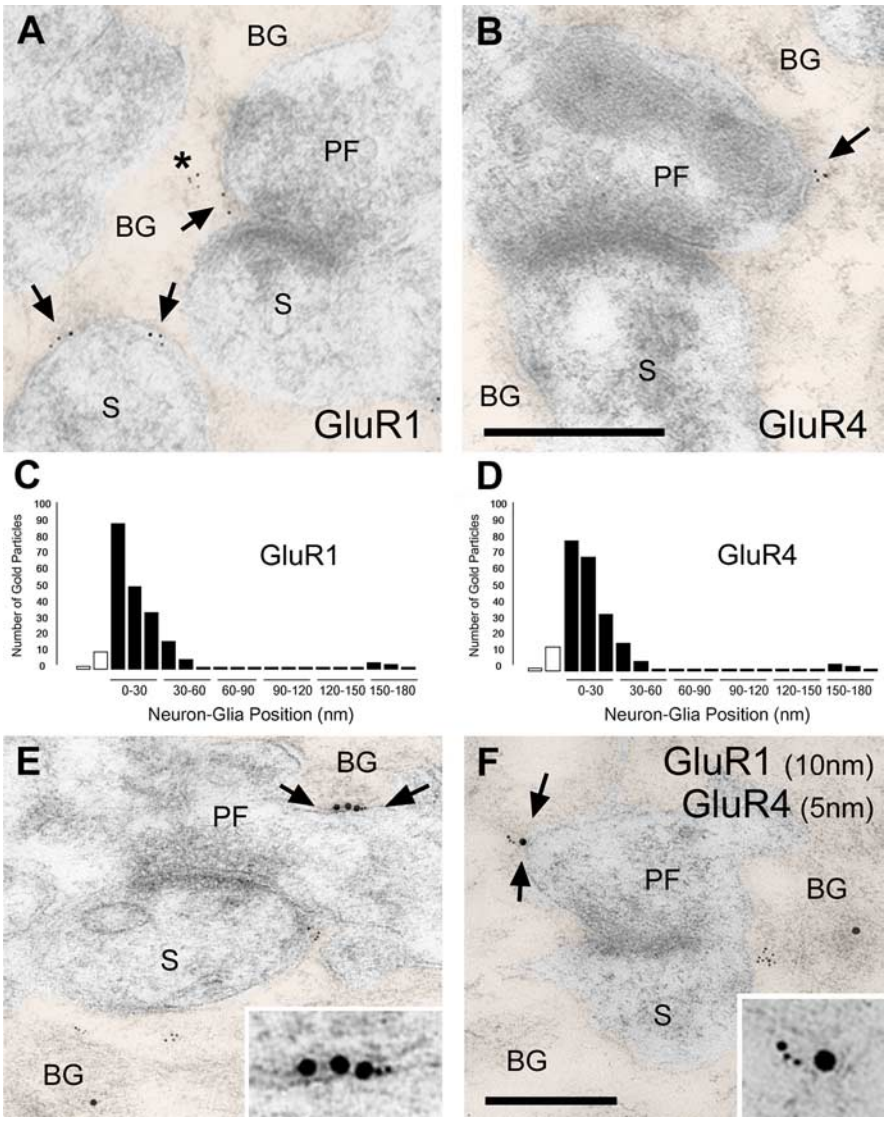

Figure 4. Immunogold labeling for GluR1 and GluR4 is associated with BGs. ***A***, Electron micrograph of a PF–PC synapse after postembedding immunogold labeling for GluR1. Gold particles are observed at the BG plasma membrane as well as intracellularly (asterisks). The arrows indicate gold particles at BG plasma membrane facing presynaptic endings (PF) or PC dendritic spines (S). BG profiles have been colorized. ***B***, Electron micrographs after postembedding immunogold labeling for GluR4. Scale bar: (in ***B***) ***A***, ***B***, 0.2 μm. ***C***, Histogram showing the position of the GluR1 gold particles relative to neuron– glia apposition. Most of the gold particles for both AMPA receptor subunits are positioned from 0 (outer leaflet of BG plasma membrane) to 40 nm toward the BG cytoplasm. White bars represent the gold particles found in the presynaptic terminal and dendritic spine. ***D***, Histogram showing the position of the GluR4 gold particles. ***E***, ***F***, GluR1 (10 nm particles) and GluR4 (5 nm particles) colocalize at the BG plasma membrane (arrows). Insets, Regions between arrows at higher magnification. Scale bar: (in ***F***) ***E***, ***F***, 0.2 μm; insets, 0.1 μm.

GluR1 and GluR4 are expressed on the membrane of BG

BG AMPA receptors are composed of GluR subunits 1 and 4; lacking GluR2, these AMPA receptors are Ca^{2+} permeable (Geiger et al., 1995). To determine the subcellular distribution of GluR1 and GluR4 in the P21 cerebellum, we performed postembedding immunogold labeling after freeze substitution (Rubio and Wenthold, 1997, 1999; Rubio and Soto, 2001). All BG profiles analyzed surrounded either CF and PF synapses in the molecular layer or PC somata located in the Purkinje cell layer. Gold particles labeling GluR1 and GluR4 were found mainly on BG (Fig. 4). Separate experiments showed that GluR2/3 labeling was found only on neurons in the cerebellum (data not shown).

Gold particles labeling GluR1 and GluR4 were found close to the plasma membranes of the soma and the processes of BG surrounding both CF and PF synapses as well as in intracellular compartments, in which they associated with cytoskeletal and/or vesicle-like structures (Figs. 4, 5). To determine whether gold particles located near the plasma membrane were associated with BGs or neurons, we measured the distribution of gold particles relative to the plasma membrane. For both AMPA receptor subunits, the majority of gold particles were located in the BG within 40 nm from the outer leaflet of the BG plasma membrane that faced the presynaptic ending or the dendritic spine (Fig. 4*C*,*D*). This distribution indicates that GluR1 and GluR4 are expressed by BGs rather than neurons.

In some cases, GluR1 and GluR4 were found colocalized by double-postembedding immunogold labeling (Fig. 4*E*,*F*). Gold particles labeling both receptor subunits were found closely associated both intracellularly and at the BG membranes facing PF

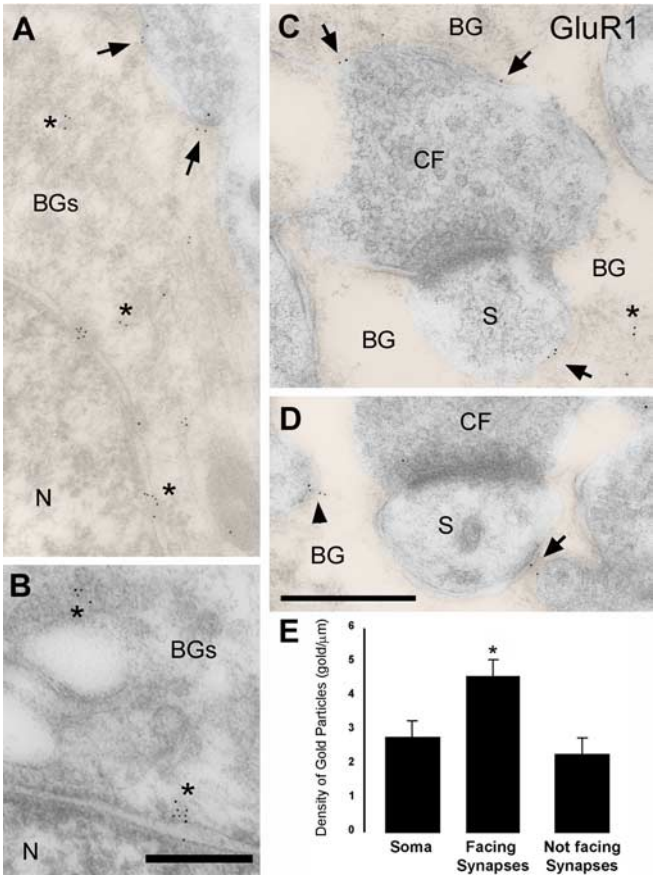

Figure 5. Densities of gold particles labeling GluR1 on the BG plasma membrane. ***A***, ***B***, Electron micrographs of BG soma after postembedding immunogold labeling for GluR1. At the BG soma, gold particles for GluR1 are associated with the plasma membrane (arrows) and intracellularly (asterisks). N, Nucleus. BG profiles in ***A***, ***C***, and ***D*** have been colorized. ***C***, ***D***, At BG processes wrapping CF synapses (CF, presynaptic ending; S, PC dendritic spines), gold particles decorate the plasma membrane facing the synapses (arrows) and the plasma membrane "not facing synapses" (arrowheads), as well as intracellularly (asterisks). Scale bars: (in ***D***) ***A***, ***C***, ***D***, 0.2 μm; ***B***, 0.1 μm. ***E***, Histogram showing the density of gold particles for GluR1 at the BG plasma membrane of the soma, BG plasma membrane facing the synapse, and BG plasma membrane not facing the synapse. Note that the density of gold particles in not facing synapses is an upper limit, because there could be synapses in other sections. Density of gold particles in membranes facing synapses was statistically different from that in the soma ($*p < 0.05$) and from that in not facing synapses membranes ($p < 0.001$). Error bars represent SE.

synapses. This suggests that heteromeric receptor complexes formed by the GluR1 and GluR4 subunits may mediate AMPA receptor currents in the BG.

Relative density of GluR1 at the soma and the membrane surrounding the synapse

We calculated the average density of gold particles for GluR1 at the plasma membrane of the BG soma and processes surrounding synapses. All gold particles within 20 nm of the outer leaflet of BG plasma membrane were counted. Because the distribution of GluR1 and GluR4 at BG membranes was essentially the same, we focused on the GluR1 distribution. Three different regions of BG plasma membrane were differentiated: the soma, membrane facing CF and PF synapses, and membrane not associated with synapses. We found gold particles at the highest density at the membrane facing the synapses (Fig. 5*E*).

Using electrophysiological techniques, we estimated the absolute density of functional AMPA receptors at the BG soma to be 47 ± 19 receptors/μm^2 (Fig. 3*C*). Assuming that the labeling efficacy is uniform across the tissue for the same preparation, we used the ratio of GluR1 gold particle density at the soma and at the membrane surrounding the synapse (1.65) to estimate the density of functional AMPA receptors at the membrane surrounding synapses (77 ± 31 receptors/μm^2) [see appendix of Takumi et al. (1999)].

Distribution of GluR1 in the membrane surrounding the synapse

We next determined whether the gold particles labeling GluR1 were differentially distributed along BG membrane facing synapses. The BG membrane area surrounding the synapse was divided into three sections: membrane surrounding the presynaptic element, membrane facing the synaptic cleft, and membrane surrounding the postsynaptic spine (Fig. 6*A*). We then calculated the density of gold particles for GluR1 in each section for both CF and PF synapses. We found that, for CF, there was little preferential distribution of GluR1 gold particles at each section (Fig. 6*B*). However, the gold particles at the BG surrounding PF were preferentially distributed at the cleft and presynaptic sections (Fig. 6*C*).

We also observed that gold particles were either isolated or in clusters of two to six gold particles at both the BG plasma membrane and intracellularly (Figs. 4, 5). Intracellular gold particles were associated with membranes of the smooth endoplasmic reticulum in the cell body and BG processes or cytoskeleton, as described previously in neurons (Rubio and Wenthold, 1999). The presence of clusters of gold particles suggests that several receptors are closely associated. We also found that small clusters (one or two gold particles) occurred more often in the membrane surrounding the PC dendritic spine, whereas larger clusters (three to six gold particles) occurred more often in the membrane surrounding the presynaptic element (Fig. 6*D*).

Structural specialization of neural–glial apposition

To estimate the P_O at the peak of BG quanta, the extent of glutamate spread after exocytosis needs to be estimated. The spatial concentration profile of glutamate from the site of vesicle fusion will depend, in part, on the width of the extracellular space between the two cells. Structural analysis of the synapse and the neural–glial apposition was performed using two different methods of fixation: immersion-fixed, epon-embedded cerebellum (Fig. 7*A*,*B*) and perfusion-fixed, Lowicryl-embedded cerebellum after freeze substitution (Fig. 7*C*,*D*). In both cases, we find that the extracellular space between presynaptic elements and apposing BG processes is narrower than the synaptic cleft by a factor of ~1.9 (Fig. 7*F*).

We also noticed that some areas of the apposition of the presynaptic and BG membranes appeared to be extremely close to each other (Fig. 7*A–D*). Such areas were accompanied by electron-dense material in the extracellular space (Fig. 7*B–D*) and sometimes with closely associated presynaptic vesicles (Fig. 7*A*,*C*). This suggests the existence of an area in which neuron to glial cell communication may occur. Because such fine structural analysis could not be done after the postembedding procedure, we do not know whether these structures colocalize with clusters of AMPA receptors. Nevertheless, the preferential distribution of gold particles for GluR1 at the BG plasma membrane surrounding the presynaptic ending (PF in particular) suggests that they contain AMPA receptors (Fig. 6).

Estimation of P_O at the peak of BG quantal response

We estimated the BG AMPA receptor density at the membrane surrounding the synapse (Figs. 3*C*, 5*E*), and we measured the peak amplitude of the quantal events (Fig. 1*E*). To calculate the P_O at the peak of BG quanta, we need to estimate the average area over which glutamate attains a concentration that is sufficient to rapidly activate AMPA receptors after release from single vesicles. To do this, we first used PC quanta to estimate the extent of glutamate spread attributable to exocytosis of single vesicles at CF to PC synapses. The number of channels opened (N_{open}) at the peak of the quantal response is given by the following:

$$N_{open} = G_{peak}/\gamma, \quad (1)$$

where G_{peak} is the peak conductance of quantal response, and γ is the single-channel conductance. G_{peak} was 872 ± 246 pS (Fig. 1*E*) ($n = 5$ cells) for CF-to-PC synapse and γ of PC AMPA receptors, measured with nonstationary noise analysis was 13.7 ± 2.5 pS ($n = 6$ patches), both in the absence of CTZ. N_{open} averaged 64 ± 21 receptors.

P_{Opeak} for quantal events at this synapse was estimated using low-affinity antagonists (Wadiche and Jahr, 2001) to be 0.27–0.39. The number of receptors exposed ($N_{exposed}$) by the bolus of glutamate is 163 ± 55 ~ 236 ± 80, as given by the following:

$$N_{exposed} = N_{open}/P_{Opeak}. \quad (2)$$

AMPA receptor density (D_{AMPA}) at the PSD of CF to PC synapses has been estimated to be 1280 receptors/μm^2 (Tanaka et al., 2005). The exposed area ($A_{exposed}$) of PC membrane to glutamate is given by the following:

$$A_{exposed} = N_{exposed}/D_{AMPA}. \quad (3)$$

Using these numbers, $A_{exposed}$ is 0.13 ± 0.04 ~ 0.18 ± 0.06 μm^2. This estimate of the spread area of glutamate with a single vesicle matches the PSD area reported in a serial EM reconstruction study (CF–PC PSD, 0.14 μm^2; PF–PC PSD, 0.13 μm^2) (Xu-Friedman et al., 2001). Matching of the $A_{exposed}$ estimate and the PSD area, coupled with the fact that P_{Omax} of PC AMPA receptors in patches reaches only ~0.66 (Wadiche and Jahr, 2001), suggests that a fairly high-concentration transient of glutamate is attained across the entire PSD after exocytosis, although certainly not completely uniform. In contrast, we have shown that evoked quantal responses in PCs were not coincident with those in BGs (Matsui and Jahr, 2003). This indicates that glutamate released from single vesicles does not spill over to the BG membrane to a significant degree. Therefore, although the spread of glutamate is not limited to the apposition between the active zone and the PSD, it seems that ~0.13–0.18 μm^2 is close to the upper limit of the area in which glutamate can diffuse at high enough concentration to activate significant numbers of low-affinity AMPA receptors.

Because we found that the intermembrane distance is narrower at the neural–glial apposition than within the synaptic cleft by a factor of ~1.9 (Fig. 7*F*), exocytosis at the neural–glial apposition will result in a greater lateral spread of glutamate than at the wider synaptic cleft. This results in $A_{exposed}$ for the BG of 0.25–0.35 μm^2. D_{AMPA} at the BG membrane surrounding the presynaptic element was estimated to be 77 receptors/μm^2. Therefore, $N_{exposed}$ at the BG membrane was 19.0–27.4 receptors, as calculated by Equation 3. G_{peak} was 288 ± 52 pS ($n = 4$ cells) and 238 ± 20 pS ($n = 7$ cells) at CF-to-BG and PF-to-BG quantal responses, respectively (Fig. 1*E*). Because γ was 26.6 ± 6.5 pS (Fig. 2*F*), using Equation 1, we calculated N_{open} to be 8.9 ± 2.3 ~ 10.8 ± 3.3 receptors. Using Equation 2, P_{Opeak} for the BG quantal event was 0.33 ± 0.19 ~ 0.57 ± 0.35. Because the glutamate transient will be nonuniform across the entire $A_{exposed}$, P_{Opeak} calculated by this method is an average value.

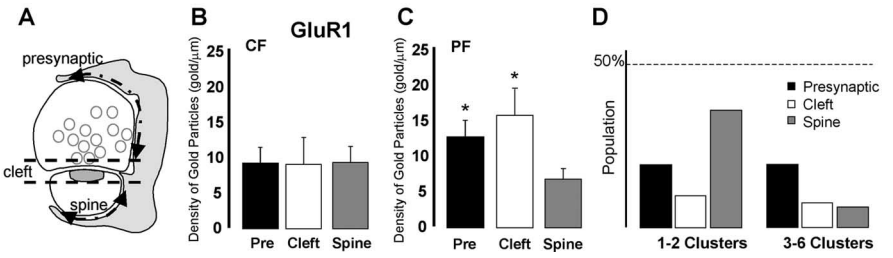

Figure 6. Distribution of GluR1 labeling on BG processes surrounding CF and PF synapses. ***A***, Schematic of a synapse surrounded by a BG process (gray). Arrows indicated the presynaptic and spine sections of the BG. The space between the dashed lines represents the synaptic cleft section of the BG process apposed to presynaptic and spine plasma membrane. Gold particles assigned to the "Cleft" category were, on average, 84 nm from the "T" intersection of the apposition between the presynaptic and postsynaptic membranes. Particles in the "Pre" category are those found along the rest of the apposition of the presynaptic bouton, whereas those in the "Spine" category are those apposing the spine up to the spine neck. ***B***, ***C***, Histograms show the density of gold particles for GluR1 at these three membrane sections surrounding CF and PF synapses. Pre, Presynaptic. *$p < 0.05$. ***D***, Histograms show the distribution of clusters of one or two and three to six gold particles labeling GluR1 on the BG membrane at the presynaptic, cleft, and spine membrane sections. The percentage of the two groups was related to the total population of gold particles ($n = 215$ gold particles). Error bars represent SE.

Simulations using kinetic model of BG AMPA receptors

Using the rise time and the P_{Opeak} of the BG quantal responses, we can estimate the amplitude of the glutamate transient with a kinetic model for BG AMPA receptors. The simple four-state model by Dzubay and Jahr (1999) was used (Fig. 8*A*), but the rate constants were somewhat different because of the constraint of P_{Omax} obtained by noise analysis (Fig. 2*E*,*F*). Desensitization states were omitted because of the use of CTZ. The dose–P_O curve (Fig. 2*B*, open circles) and the dose–rise time curve (Fig. 2*D*, open circles) to steps of various concentrations of glutamate were reasonably well fitted with the model, although the rise time of the patch response for the 100 μM glutamate pulse was slower than the model prediction. This suggests that the simple four-state model is not adequate to describe the behavior of the BG AMPA receptors over the full range of glutamate concentrations. We used this simple model, because it can simulate the response to the higher-concentration transients of glutamate, which are relevant in this study.

This model was then driven with various glutamate transients with instantaneous rise times and exponential decay times (Fig. 8*B*). Noninstantaneous rise of the glutamate transient with values up to approximately one-half of the decay time constant had negligible effect on the resulting rise time or the P_{Opeak} of the response within the range that we studied (data not shown). The rise time of the simulated response was plotted against the peak amplitude of the glutamate transient using decay times of the glutamate transient from 0.1 to 1.0 ms (Fig. 8*D*). The quantal event rise times of 192–224 μs are indicated by the dashed lines in the figure and show the limited range of concentration and decay times that are feasible. Very rapid decaying transients (0.1 ms)

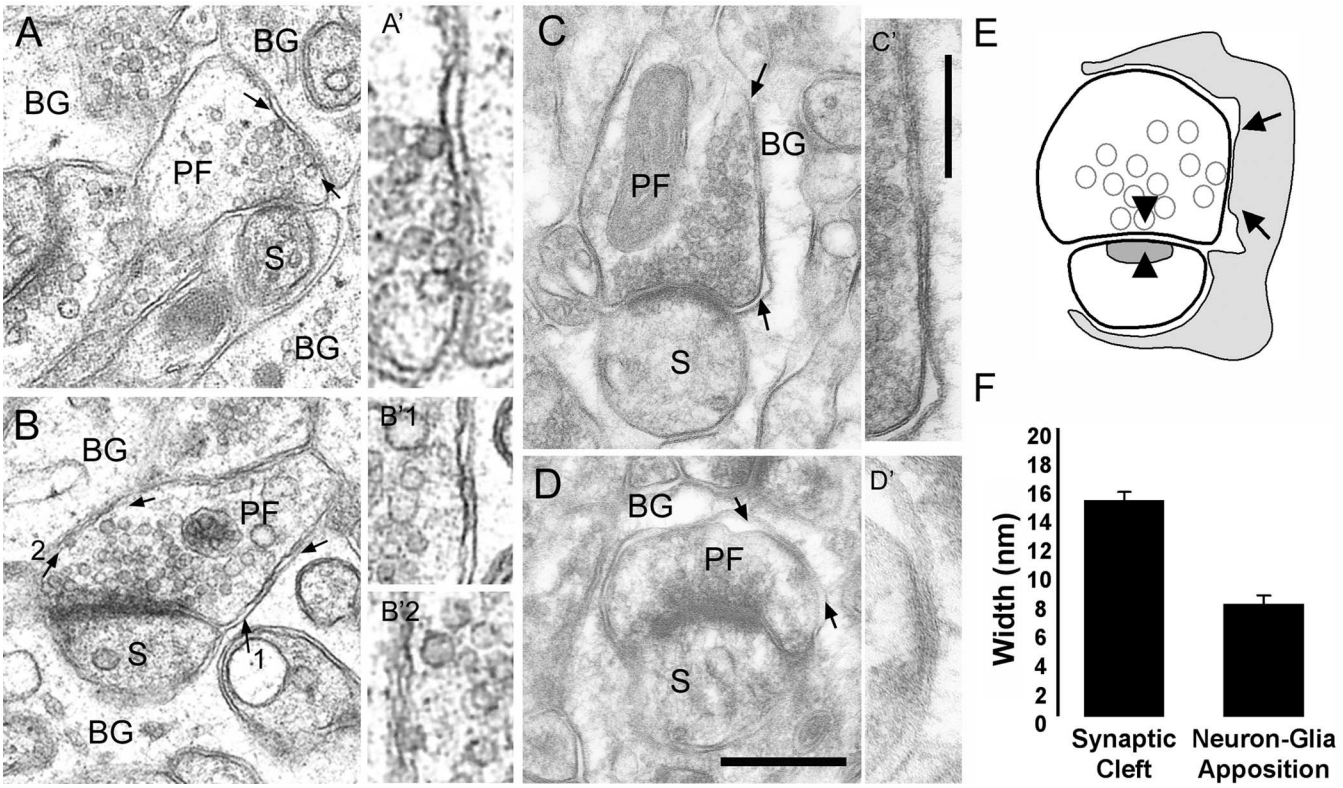

Figure 7. Close apposition between the BG and PF bouton plasma membranes. ***A***, ***B***, Electron micrographs showing immersion-fixed, epon-embedded cerebellum. ***A***, Synaptic vesicles docked to the presynaptic membrane specialization and to the PF membrane facing the BG membrane (arrows). ***A′***, Magnification of membrane apposition in ***A***, indicated by arrows. ***B***, Close apposition of PF and BG plasma membranes containing extracellular electron-dense material (arrows). ***B′1***, ***B′2***, Magnified areas of ***B***, indicated by arrows. ***C***, ***D***, Lowicryl-embedded cerebellum after freeze substitution. Arrows indicate PF–BG close membrane appositions with electron-dense extracellular material. ***C***, Synaptic vesicles are docked to the presynaptic specialization and close to the presynaptic membrane facing the BG. ***C′–D′***, Insets, A higher magnification of the area between arrows. Scale bars: (in ***D***) ***A–D***, 0.2 μm; (in ***C′***) ***A′–D′***, 0.1 μm. ***E***, Schematic drawing shows a PF-PC synapse surrounded by BG processes (gray). Arrowheads indicate the presynaptic and postsynaptic specialization (cleft), and arrows represent the closest apposition of the BG and PF plasma membrane. ***F***, Histogram of the distance between the presynaptic and postsynaptic membrane (synaptic cleft) and between BG and neuronal (presynaptic ending and dendritic spine) plasma membranes. S, PC dendritic spines. Error bars represent SE.

produce event rise times that are too fast. However, the decay time constant of the quantal events (from CF, 1.1 ± 0.1 ms, n = 4 cells; from PF, 1.4 ± 0.1 ms, n = 7 cells) was similar to the deactivation rate of the receptor (1.3 ± 0.2 ms; n = 24 patches), indicating that the glutamate transient decays fairly rapidly and does not control the quantal decay rate.

The P_{Opeak} of the simulated response was also plotted against the peak amplitude of the glutamate transient with various decay times of the glutamate transient (Fig. 8*E*). Using calculations described in the previous section, P_{Opeak} for the BG quantal response was estimated as 0.33–0.57. Low concentrations and very rapid transients of glutamate could not produce such a high P_{Opeak}. Therefore, to satisfy both the rise time measurements and the P_{Opeak} estimates of BG quantal responses, the glutamate transient has to have a high-concentration peak (1.0–1.5 mM) and rapid decay time constant (Fig. 8*D*,*E*, circled points) (~0.5 ms).

The glutamate transient underlying the BG quanta is likely to have an amplitude in the millimolar range, similar to the concentration thought to occur at the PSD just across from the presynaptic active zone (Clements, 1996; Diamond and Jahr, 1997; Wadiche and Jahr, 2001). Theoretical estimates of the peak glutamate concentration resulting from spillover at more distant sites are much lower (Rusakov et al., 1999; Barbour, 2001). The estimate of the glutamate concentration, therefore, supports the idea that quanta recorded in BGs are not the result of spillover, but rather are caused by direct release onto the BG membrane from ectopic presynaptic sites. Neural–glial communication via ectopic release is probably necessary to rapidly activate the low-affinity, Ca^{2+}-permeable AMPA receptors expressed by BGs.

Discussion

Discrepancy between theoretical and experimental estimates of spillover

Most diffusion models predict that the extrasynaptic concentrations of transmitter attained by diffusion out of the cleft are relatively small (Eccles and Jaeger, 1958; Barbour, 2001; Franks et al., 2003). High concentrations of transmitter are thus assumed to be confined to the synaptic cleft, and transmitter does not spillover to neighboring structures. In contrast, others predict significant spillover (Rusakov et al., 1999). These disparate conclusions depend on the values of the diffusion coefficient of glutamate in extracellular space and the number of transmitter molecules contained in a synaptic vesicle, neither of which are well defined experimentally. In contrast, a number of experimental observations support the idea that transmitter can spread to extrasynaptic receptors, surrounding glial membrane, or even to neighboring synapses (Trussell et al., 1993; Bergles et al., 1997; DiGregorio et al., 2002; Xu-Friedman and Regehr, 2003). One remedy for the estrangement between simulated and experimental observations is ectopic release, in which vesicles are released at some distance from the conventional synaptic active zone. Ectopic release produces high concentrations of transmitter out-

side of the synaptic cleft. The existence of such ectopic release has been suggested by freeze-fracture studies of the neuromuscular junction (Ceccarelli et al., 1979, 1988), FM1-43 [*N*-(3-triethylammoniumpropyl)-4-(4-(dibutylamino)styryl) pyridinium dibromide] imaging studies of retinal bipolar cells (Zenisek et al., 2000, 2003), ultrastructural studies of hair cells (Lenzi et al., 2002), and electrophysiological recordings of transmission between CFs and BGs (Matsui and Jahr, 2003, 2004).

Discrepancy between the concentration estimates at BG AMPA receptors

Previous estimates of glutamate transients at BG AMPA receptors after CF stimulation (~200 μM) (Bergles et al., 1997; Dzubay and Jahr, 1999) are lower than the present value. There are several reasons for this discrepancy. Bergles et al. (1997) compared the rise time of the evoked response with the rise time of the patch response to estimate the peak glutamate concentration. Because the synaptically evoked response is the sum of many quantal events, release asynchrony after action potential invasion will slow the evoked responses and result in an underestimate of the glutamate concentration. By using quantal events, the present study avoids the ambiguity introduced by release asynchrony.

Dzubay and Jahr (1999) estimated the size of the glutamate transient by measuring the potentiation of the evoked response by CTZ, which increases the apparent affinity of AMPA receptors for glutamate by approximately sixfold. Based on our more recent studies (Wadiche and Jahr, 2001; Matsui and Jahr, 2003, 2004) and the work presented here, we now interpret the enhancement by CTZ differently. In normal levels of extracellular Ca^{2+}, CF stimulation results in multivesicular release at individual synapses (Wadiche and Jahr, 2001; Foster et al., 2002; Foster and Regehr, 2004) and significant diffusion of glutamate out of the cleft (Matsui and Jahr, 2004). Even with this heightened spillover of glutamate, the low-affinity BG AMPA receptors are predominantly activated by the much larger local concentration transients caused by ectopic release (Matsui and Jahr, 2004). In the presence of CTZ, however, spillover activates many more AMPA receptors than in control as a result of their sixfold higher affinity. This, in turn, greatly increases the evoked response.

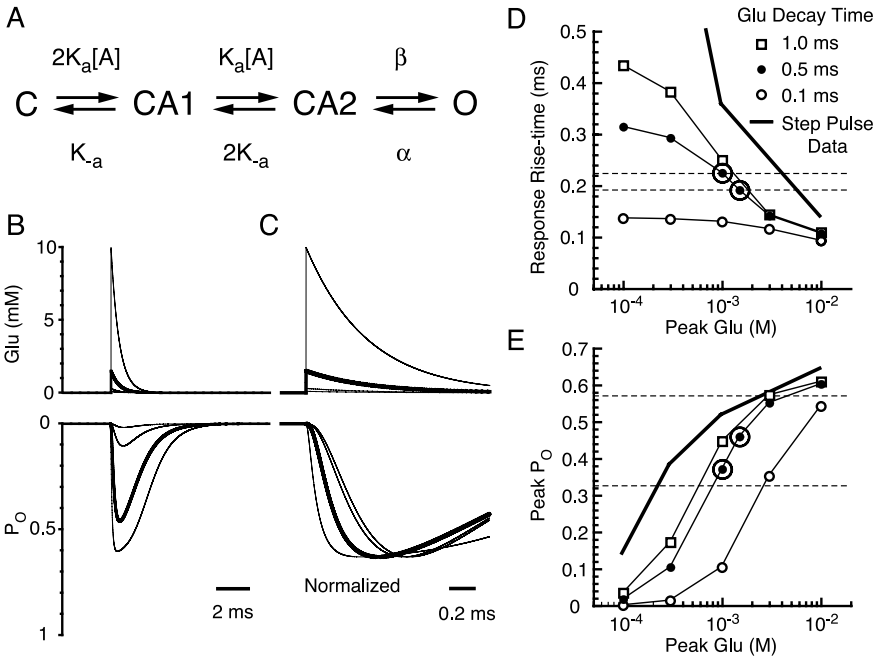

Figure 8. Simulation of AMPA receptor kinetics. ***A***, Kinetic scheme of the AMPA receptor model used to fit AMPA receptor currents in outside-out patches. Two equal binding sites for glutamate are assumed. Four parameters were manually iterated to fit the P_0 and the kinetics of glutamate response in conventional outside-out patches as in Figure 2. Rates used were as follows (units are per molar per second for K_a or per second for the rest): $K_a = 7.5 \times 10^6$, $K_{-a} = 1.6 \times 10^3$, $\beta = 8.2 \times 10^3$, and $\alpha = 4.9 \times 10^3$. ***B***, The model was driven with glutamate transients with an instant rise and single exponential decay with a time constant of 0.5 ms and variable peak amplitude (top). The resulting simulated response is shown below. Thick traces show glutamate transient with peak of 1.5 mM and the simulated response. ***C***, The same traces as in ***B***, with simulated responses normalized to their peak amplitudes and shown in an expanded time scale. ***D***, Rise time (20–80%) of the simulated AMPA receptor responses versus peak glutamate concentration with various decay time constants of the glutamate transient (as indicated). The thick line indicates the average rise time of patches to step increases of glutamate (from Fig. 2*D*). Two horizontal dashed lines indicate the average rise times of the quanta recorded by CF (bottom) or PF (top) stimulation. ***E***, Peak P_0 of the simulated AMPA receptor response versus peak glutamate concentration. The thick line indicates the P_0 of patch responses to step increases of glutamate (from Fig. 2*B*). Horizontal lines indicate the range of P_0 estimated in the text. Symbols are the same as in ***D***. Large open circles in ***D*** and ***E*** indicate optimum points (peak glutamate concentration, 1–1.5 mM; decay time, 0.5 ms) that satisfy both the kinetic and P_{0peak} requirements.

Why is ectopic release necessary?

Unlike spillover, which results in lower concentrations of glutamate at the BG membrane, ectopic release produces a very high concentration that rapidly activates nearby low-affinity AMPA receptors ($EC_{50} > 1$ mM without CTZ). Few of these AMPA receptors would be likely to open if not for nearby ectopic release. Ca^{2+} influx through these AMPA receptors may be required for the encasement of PC synapses by BG membrane (Iino et al., 2001). Ectopic release may provide a geographical cue to guide BG membranes to surround active synapses and ensure efficient uptake of glutamate that diffuses out of the synaptic cleft.

Paired recordings from PCs and BGs show that monovesicular release of glutamate into the cleft does not result in spillover sufficient for activating BG AMPA receptors even in the presence of CTZ (Matsui and Jahr, 2003). Based on our simulations, this suggests that the glutamate concentration resulting from spillover does not reach ~100 μM at BG AMPA receptors. If monovesicular release is the usual mode of release from presynaptic elements, ectopic release may be necessary to activate receptors beyond the reach of spillover.

Distribution of BG AMPA receptors

A combination of electrophysiological recordings and quantitative immunogold EM analysis has allowed us to quantify the distribution of AMPA receptors in BGs. AMPA receptor density in BG somata is much higher than that in PC somata (~17-fold). In contrast, the difference in the density of AMPA receptors at the BG somatic membrane and the membrane surrounding synapses is not large (~1.65-fold). Thus, the membrane specialization at the neural–glial apposition is not nearly as dramatic as that at the neuronal postsynaptic density, where a very high density of AMPA receptors is observed (~1000 receptors/μm^2) (Momiyama et al., 2003; Tanaka et al., 2005). Such relatively uniform and modest densities of AMPA receptors throughout the BG membrane may allow these cells to sense ectopic release that may not occur at stationary sites but rather may occur more randomly

in the presynaptic element (Zenisek et al., 2000). Alternatively, clustering of BG AMPA receptors and areas of close apposition of presynaptic and BG membranes may mark more permanent sites of ectopic release.

References

Altman J, Bayer SA (1997) Development of cerebellar system in relation to its evolution, structure and functions. New York: CRC.

Araque A, Carmignoto G, Haydon PG (2001) Dynamic signaling between astrocytes and neurons. Annu Rev Physiol 63:795–813.

Atluri PP, Regehr WG (1998) Delayed release of neurotransmitter from cerebellar granule cells. J Neurosci 18:8214–8227.

Barbour B (2001) An evaluation of synapse independence. J Neurosci 21:7969–7984.

Bergles DE, Dzubay JA, Jahr CE (1997) Glutamate transporter currents in Bergmann glial cells follow the time course of extrasynaptic glutamate. Proc Natl Acad Sci USA 94:14821–14825.

Bezzi P, Volterra A (2001) A neuron-glia signalling network in the active brain. Curr Opin Neurobiol 11:387–394.

Ceccarelli B, Grohovaz F, Hurlbut WP (1979) Freeze-fracture studies of frog neuromuscular junctions during intense release of neurotransmitter. II. Effects of electrical stimulation and high potassium. J Cell Biol 81:178–192.

Ceccarelli B, Fesce R, Grohovaz F, Haimann C (1988) The effect of potassium on exocytosis of transmitter at the frog neuromuscular junction. J Physiol (Lond) 401:163–183.

Clark BA, Barbour B (1997) Currents evoked in Bergmann glial cells by parallel fibre stimulation in rat cerebellar slices. J Physiol (Lond) 502:335–350.

Clements JD (1996) Transmitter timecourse in the synaptic cleft: its role in central synaptic function. Trends Neurosci 19:163–171.

Diamond JS, Jahr CE (1997) Transporters buffer synaptically released glutamate on a submillisecond time scale. J Neurosci 17:4672–4687.

DiGregorio DA, Nusser Z, Silver RA (2002) Spillover of glutamate onto synaptic AMPA receptors enhances fast transmission at a cerebellar synapse. Neuron 35:521–533.

Duan S, Anderson CM, Stein BA, Swanson RA (1999) Glutamate induces rapid upregulation of astrocyte glutamate transport and cell-surface expression of GLAST. J Neurosci 19:10193–10200.

Dzubay JA, Jahr CE (1999) The concentration of synaptically released glutamate outside of the climbing fiber-Purkinje cell synaptic cleft. J Neurosci 19:5265–5274.

Eccles JC, Jaeger JC (1958) The relationship between the mode of operation and the dimensions of the junctional regions at synapses and motor end-organs. Proc R Soc Lond B Biol Sci 148:38–56.

Foster KA, Regehr WG (2004) Variance-mean analysis in the presence of a rapid antagonist indicates vesicle depletion underlies depression at the climbing fiber synapse. Neuron 43:119–131.

Foster KA, Kreitzer AC, Regehr WG (2002) Interaction of postsynaptic receptor saturation with presynaptic mechanisms produces a reliable synapse. Neuron 36:1115–1126.

Franks KM, Stevens CF, Sejnowski TJ (2003) Independent sources of quantal variability at single glutamatergic synapses. J Neurosci 23:3186–3195.

Geiger JR, Melcher T, Koh DS, Sakmann B, Seeburg PH, Jonas P, Monyer H (1995) Relative abundance of subunit mRNAs determines gating and Ca^{2+} permeability of AMPA receptors in principal neurons and interneurons in rat CNS. Neuron 15:193–204.

Grosche J, Matyash V, Moller T, Verkhratsky A, Reichenbach A, Kettenmann H (1999) Microdomains for neuron-glia interaction: parallel fiber signaling to Bergmann glial cells. Nat Neurosci 2:139–143.

Hille B (2001) Ionic channels of excitable membranes, p 397. Sunderland, MA: Sinauer.

Iino M, Goto K, Kakegawa W, Okado H, Sudo M, Ishiuchi S, Miwa A, Takayasu Y, Saito I, Tsuzuki K, Ozawa S (2001) Glia-synapse interaction through Ca2+-permeable AMPA receptors in Bergmann glia. Science 292:926–929.

Karpen JW, Loney DA, Baylor DA (1992) Cyclic GMP-activated channels of salamander retinal rods: spatial distribution and variation of responsiveness. J Physiol (Lond) 448:257–274.

Koh DS, Geiger JR, Jonas P, Sakmann B (1995) Ca(2+)-permeable AMPA and NMDA receptor channels in basket cells of rat hippocampal dentate gyrus. J Physiol (Lond) 485:383–402.

Lenzi D, Crum J, Ellisman MH, Roberts WM (2002) Depolarization redistributes synaptic membrane and creates a gradient of vesicles on the synaptic body at a ribbon synapse. Neuron 36:649–659.

Matsui K, Jahr CE (2003) Ectopic release of synaptic vesicles. Neuron 40:1173–1183.

Matsui K, Jahr CE (2004) Differential control of synaptic and ectopic vesicular release of glutamate. J Neurosci 24:8932–8939.

Momiyama A, Silver RA, Hausser M, Notomi T, Wu Y, Shigemoto R, Cull-Candy SG (2003) The density of AMPA receptors activated by a transmitter quantum at the climbing fibre-Purkinje cell synapse in immature rats. J Physiol (Lond) 549:75–92.

Mugnaini E (1972) The histology and cytology of the cerebellar cortex. In: The comparative anatomy and histology of the cerebellum: the human cerebellum, cerebellar connections, and cerebellar cortex (Larsell O, Jansen J, eds), pp 201–251. Minneapolis: University of Minnesota.

Newman EA (2001) Propagation of intercellular calcium waves in retinal astrocytes and Muller cells. J Neurosci 21:2215–2223.

Palay SL, Chan-Palay V (1974) Cerebellar cortex. New York: Springer.

Peters A, Palay SL, Webster H de F (1991) The fine structure of the nervous system. Neurons and their supporting cells. New York: Oxford UP.

Porter JT, McCarthy KD (1996) Hippocampal astrocytes in situ respond to glutamate released from synaptic terminals. J Neurosci 16:5073–5081.

Rubio ME, Soto F (2001) Distinct localization of P2X receptors at excitatory postsynaptic specializations. J Neurosci 21:641–653.

Rubio ME, Wenthold RJ (1997) Glutamate receptors are selectively targeted to postsynaptic sites in neurons. Neuron 18:939–950.

Rubio ME, Wenthold RJ (1999) Differential distribution of intracellular glutamate receptors in dendrites. J Neurosci 19:5549–5562.

Rusakov DA, Kullmann DM, Stewart MG (1999) Hippocampal synapses: do they talk to their neighbours? Trends Neurosci 22:382–388.

Sather W, Dieudonne S, MacDonald JF, Ascher P (1992) Activation and desensitization of *N*-methyl-D-aspartate receptors in nucleated outside-out patches from mouse neurones. J Physiol (Lond) 450:643–672.

Sigworth FJ (1980) The variance of sodium current fluctuations at the node of Ranvier. J Physiol (Lond) 307:97–129.

Takayama C, Nakagawa S, Watanabe M, Mishina M, Inoue Y (1996) Developmental changes in expression and distribution of the glutamate receptor channel delta 2 subunit according to the Purkinje cell maturation. Brain Res Dev Brain Res 92:147–155.

Takumi Y, Ramirez-Leon V, Laake P, Rinvik E, Ottersen OP (1999) Different modes of expression of AMPA and NMDA receptors in hippocampal synapses. Nat Neurosci 2:618–624.

Tanaka J, Matsuzaki M, Tarusawa E, Momiyama A, Molnar E, Kasai H, Shigemoto R (2005) Number and density of AMPA receptors in single synapses in immature cerebellum. J Neurosci 25:799–807.

Trussell LO, Zhang S, Raman IM (1993) Desensitization of AMPA receptors upon multiquantal neurotransmitter release. Neuron 10:1185–1196.

Wadiche JI, Jahr CE (2001) Multivesicular release at climbing fiber-Purkinje cell synapses. Neuron 32:301–313.

Wenthold RJ, Yokotani N, Doi K, Wada K (1992) Immunochemical characterization of the non-NMDA glutamate receptor using subunit-specific antibodies. J Biol Chem 267:501–507.

Xu-Friedman MA, Regehr WG (2000) Probing fundamental aspects of synaptic transmission with strontium. J Neurosci 20:4414–4422.

Xu-Friedman MA, Regehr WG (2003) Ultrastructural contributions to desensitization at cerebellar mossy fiber to granule cell synapses. J Neurosci 23:2182–2192.

Xu-Friedman MA, Harris KM, Regehr WG (2001) Three-dimensional comparison of ultrastructural characteristics at depressing and facilitating synapses onto cerebellar Purkinje cells. J Neurosci 21:6666–6672.

Zenisek D, Steyer JA, Almers W (2000) Transport, capture and exocytosis of single synaptic vesicles at active zones. Nature 406:849–854.

Zenisek D, Davila V, Wan L, Almers W (2003) Imaging calcium entry sites and ribbon structures in two presynaptic cells. J Neurosci 23:2538–2548.

Zhang JM, Wang HK, Ye CQ, Ge W, Chen Y, Jiang ZL, Wu CP, Poo MM, Duan S (2003) ATP released by astrocytes mediates glutamatergic activity-dependent heterosynaptic suppression. Neuron 40:971–982.

Zhao HM, Wenthold RJ, Petralia RS (1998) Glutamate receptor targeting to synaptic populations on Purkinje cells is developmentally regulated. J Neurosci 18:5517–5528.